Change detection in multiple-temporal Synthetic Aperture Radar images based on averaged heterogeneous factors of neighbourhood areas

1st An Hung Nguyen
Le Quy Don Technical University
Hanoi, Vietnam
hungan@lqdtu.edu.vn

2nd Phat Tien Nguyen
Le Quy Don Technical University
Hanoi, Vietnam
nguyenphat@lqdtu.edu.vn

***Abstract*—Change detection in multiple-temporal Synthetic Aperture Radar images has been received great interests for recent decades. The basic principle of change detection is to analyse the difference images generated from two Synthetic Aperture Radar images captured in the same geographic area at two different times. The popular operators used to create difference images are traditional subtraction, ratio, logarithm based ones and modified versions of them, which can use pixel information in the local or global areas. A challenge in detecting changes is to reduce impacts of speckle noises inherently existing in Synthetic Aperture Radar images on the accuracy of the detection. This paper proposed a novel algorithm to create the difference images based on averaging heterogeneous factors of corresponding neighbourhood areas in the two images. The resultant difference image is then filtered by the average filter to reject remaining speckle noises.**

***Index Terms*—Synthetic aperture radar images, difference images, speckle noise, change detection, heterogeneous factor.**

I. Introduction and relate work

Change detection in multiple-temporal images was widely applied in practice such as management and supervision of resource and environment, search and rescue activities on river, sea and land, and etc [1] [2] [3] [4] [5] [6]. In such applications, the optical and Synthetic Aperture Radar (SAR) remote sensing images are very popularly used. However, the quality of optical images depends on weather conditions in which they are captured. For instance, their quality is poor when the weather is cloudy, or fogy, or hazy or rainy. In addition, they can not be taken at night. In comparison with optical images, quality of SAR images is hardly dependent on weather conditions and even both night and daytime. Therefore, detection of changes in multiple-temporal SAR images has recently received great interests [7] [8].

In order to detect changes, a difference image (DI) is generated from two multiple-temporal images. Pixels in the difference image are then classified into two groups: changed and unchanged. Thresholding is one of the most used classification techniques because of its simplicity. The basic principle of the thresholding methods such as Otsu [9] and Kittler-Illingworth [10] algorithms is to compute an optimal threshold for direct classification.

The first classical solution of creating the DI image was to subtract two multiple-temporal images or to take the ratio of them [11] [12]. Because the nature of speckle noises in SAR images is multiplicative, ratio based operators are more usually used instead of the subtraction. From these ratio operators, there are many their modified versions developed to improve ability of removing speckle noises and accuracy of change detection. This section revises these operators for developing a novel solution of DI image creation.

Let us assume two images I_1, I_2 to be two SAR images captured in the same place at two different times. The popular operator is a ratio one, which is defined as follows.

$$I_R(x,y) = \frac{I_1(x,y)}{I_2(x,y)} \tag{1}$$

where $I_R(x,y)$ is a ratio of pixel intensities of images I_1 and I_2 on the positions of x and y.

For change detection using the ratio operator, the following rule was used. If $I_R(x,y)$ is equal to 1, it means there is no change. Otherwise, if $I_R(x,y)$ is different to 1, it means there is a change. In other words, changes occur when $I_1(x,y)$ is larger or less than $I_2(x,y)$. Therefore, there are two thresholds to build the change map from the ratio operator. For the simplification in building the change map, the single-threshold approach [13] was proposed as follows.

$$I_{STR}(x,y) = 1 - \frac{min(I_1(x,y), I_2(x,y))}{max(I_1(x,y), I_2(x,y))} \tag{2}$$

If there is no change at the position with the coordinates of x and y, $min(I_1(x,y), I_2(x,y))$ is equal to $max(I_1(x,y), I_2(x,y))$, so $I_{STR}(x,y)$ is equal to 0. Otherwise, $I_{STR}(x,y)$ is less than 1, it means there is a change.

Because speckle noises, which inherently exist in SAR images, affect accuracy of change detection, limiting their impacts has been received a great interest in the change detection task. Based on the multiplicative nature of speckle noises and the multiplication property of logarithm operation,

978-1-6654-1001-4/21/$31.00 ©2021 IEEE

the logarithm ratio (LR) operator was proposed [14]. For instance, it is defined as following:

$$I_{LR}(x,y) = ln\frac{I_1(x,y)}{I_2(x,y)} \tag{3}$$

For this operator, the multiplicative noise is transformed into additive one, and it is convenient to be dealt with. With this operator, there is no change when $I_1(x,y)$ and $I_2(x,y)$ are equal together, it means $I_{LR}(x,y)$ equals 0. Otherwise, $I_{LR}(x,y)$ is different to 0; however, value range of DI images generated by the LR operator is considerably smaller than that of the ratio operator.

The three above considered operators only take intensity information of each pixel. They can reduce more influence of speckle noises when exploiting information of neighbourhoods. From that, the ratio operator based on the neighbourhood mean was developed. The mathematical formula of this operator was defined as follows.

$$I_{NMR}(x,y) = 1 - \frac{min(u_1(x,y), u_2(x,y))}{max(u_1(x,y), u_2(x,y))} \tag{4}$$

where $u_1(x,y)$ and $u_2(x,y)$ are the means of local areas with considered pixels $I_1(x,y)$ and $I_2(x,y)$ being located in the centre of the areas, respectively. With this operator, speckle noises in the two images are reduced. However, using mean operation results in the fact that the entire neighbour area is smoothed. Therefore, the neighbour area selected too large can result in loosing change information or can not preserve details of the area. Gong et al. [15] proposed an neighbourhood based ratio (NR) operator to generate the DI image. This operator was defined by (5).

$$I_{NR}(x,y) = \partial \times \frac{min(I_1(x,y), I_2(x,y))}{max(I_1(x,y), I_2(x,y))} + (1-\partial) \times \frac{\sum_{(i,j)\in\Omega_{xy}\wedge(i,j)\neq(x,y)} min(I_1(i,j), I_2(i,j))}{\sum_{(i,j)\in\Omega_{xy}\wedge(i,j)\neq(x,y)} max(I_1(i,j), I_2(i,j))} \tag{5}$$

where, Ω_{xy} is a neighbour area of pixel (x,y). $I_1(i,j)$ and $I_2(i,j)$ are respectively pixels in Ω_{xy} of two images I_1 and I_2. $\partial = \sigma(x,y)/u(x,y)$, in which $\sigma(x,y)$ and $u(x,y)$ are standard deviation and mean of Ω_{xy}, respectively. ∂ provides information of heterogeneity of Ω_{xy}, which is called the heterogeneous coefficient for convenience. For instance, the high value of ∂ is corresponding to the heterogeneous area, while its low value corresponds to the homogeneous one. The limitation of this method is that the parameter ∂ should be only in the interval [0,1]. Because if ∂ is larger than 1, then 1- ∂ is less than 0. As a result, $I_{NR}(x,y)$ can be less than 0, this seems to be unsuitable for the difference image values. From this limitation, the paper proposed a novel solution with considering two different values of heterogeneous factors which were directly calculated from the two investigated images.

The remainder of this paper is organized as follows. Section II presents the methodology and procedures of implementing the proposed algorithm. In Section III, we present some simulation results to evaluate the performance of the proposed method in the comparison with the neighbourhood based ratio (NR) algorithm [15]. In Section IV, we draw conclusions from the evaluation results and outline the related research fields in the future.

II. Proposed method

The proposed method was developed from the NR algorithm [15] whose difference image operator is described by (5). The difference of the proposed method with the NR algorithm is to use the average value of two heterogeneous factors directly calculated from two corresponding neighbourhood areas in the two investigated images instead of using one heterogeneous factor as seen in (5).

Therefore, the proposed operator based on the averaged heterogeneous factors was defined by (6).

$$I_{AHF}(x,y) = \frac{\partial_1 + \partial_2}{2} \times \frac{min(I_1(x,y), I_2(x,y))}{max(I_1(x,y), I_2(x,y))} + |1 - \frac{\partial_1 + \partial_2}{2}| \times \frac{\sum_{(i,j)\in\Omega_{xy}\wedge(i,j)\neq(x,y)} min(I_1(i,j), I_2(i,j))}{\sum_{(i,j)\in\Omega_{xy}\wedge(i,j)\neq(x,y)} max(I_1(i,j), I_2(i,j))} \tag{6}$$

where ∂_1 and ∂_2 are respectively heterogeneous factors of two corresponding neighbourhood areas of pixels $I_1(x,y)$ and $I_2(x,y)$ in the two investigated images I_1 and I_2; while the other variables and symbols in (6) were explained with the same meaning as in (5). The absolute value notation $|\bullet|$ in (6) ensures the pixel intensity of the difference image larger than 0.

Because the proposed method was based on averaging two heterogeneous factors, it was called the averaged heterogeneous factor (AHF) method for convenience. Through our experiments, it is a fact that the speckle noises still exist in the resultant difference images. Therefore, the average filters were proposed to be applied for the difference images created by the AHF method to reduce these noises.

The procedure for implementing the proposed algorithm consists of four following steps.

- **Step 1**: Create the ratio image. The ratio image (I_R) was calculated from the two multiple-temporal images, I_1 and I_2 as follows. $I_R = min(I_1, I_2)/max(I_1, I_2)$
- **Step 2**: Create the image patches and compute their heterogeneous factors. For each image pixel with the coordinates of x and y in the two images, I_1 and I_2, the respective image patches I_{p1} and I_{p2} with the size of $ns \times ns$ pixels and the considered pixel located at the centre were created. Then, the means, m_1 and m_2, and standard deviations, sd_1 and sd_2, of these two respective image patches, I_{p1} and I_{p2} were computed. From these computed parameters, the heterogeneous factors, ∂_1 and ∂_2, of the two respective image patches, I_{p1} and I_{p2} were determined as following: $\partial_1 = m_1/sd_1$ and $\partial_2 = m_2/sd_2$.
- **Step 3**: Create the difference image. All pixels in the different image I_{AHF} were defined by using the equation (6). For observation convenience, the different image

I_{AHF} was transformed into the black-white image I_{bw} by comparing the pixels of I_{AHF} with a certain threshold T, which is defined by the Kittler algorithm [10] applied on the image I_{AHF}. For instance, if the pixel $I_{AHF}(x, y)$ is less than or equal to T, the pixel $I_{bw}(x, y)$ is assigned as 0 (corresponding to the unchanged pixel or black pixel), else the pixel $I_{bw}(x, y)$ is assigned as 255 (corresponding to the changed pixel or white pixel).

- **Step 4**: Filter the back-white image I_{bw}. The average filter was applied to this image to reject remaining speckle noises. The result of this final step is the change map, in which the white pixels present changes and the black pixels describe no-change.

III. Simulation results and discussion

To simulate and evaluate the performance of the proposed method, the paper used two datasets shown in Fig. 1 and Fig. 2. The first dataset is two original multiple-temporal images of San Francisco acquired by the ERS-2 SAR sensor in 2003 and 2004 (Fig. 1(a) and (b)), and the changed map (Fig. 1(c)) obtained by integrating prior information with photo interpretation. These images have the size of 7749×7713 pixels. For simple computation, their two corresponding sections with the size of 256 $\times$ 256 pixels were investigated. The second dataset is the images of the Bern city captured before and after a flood in 1999 (Fig. 2(a) and (b)), and the changed map (Fig. 2(c)). The section of the images of the second dataset used for the simulation has the size of 301 $\times$ 301 pixels. The two above changed maps were used as reference images for evaluating the performance of the investigated algorithms, which were also called the ground truth images.

The performance evaluation of the proposed method was implemented in comparison with the neighbourhood based ratio (NR) method [15] in terms of the coefficient of percentage correct classification (PCC).

$$PCC = \frac{N - OE}{N} \times 100 \tag{7}$$

where: N is the total pixels in the ground truth image, OE is the overall error, which is summation of the number of false negative pixels (FN) and the number of false positive pixels (FP). FN is the number of changed pixels in the ground truth image wrongly classified as unchanged ones. FP is the number of unchanged pixels in the ground truth image but wrongly classified as changed ones. These numbers were calculated by comparing the resultant simulation images with the corresponding ground truth images pixel by pixel.

The simulation procedure consists of two steps. In the first step, the different neighbourhood sizes were investigated to find out the optimal neighbourhood size according to the criteria of PCC. In the second step, for each neighbourhood size applied in the first step, the proposed method was performed with using the average filters with different sizes applied to the result image. From that the optimal combination of the filter sizes and the neighbourhood sizes for the same criteria was determined.

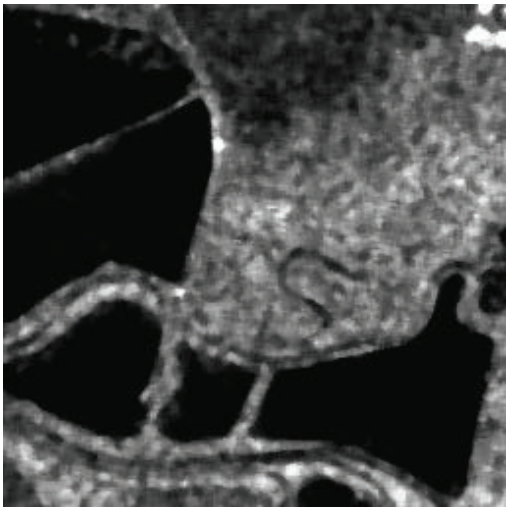

(a)

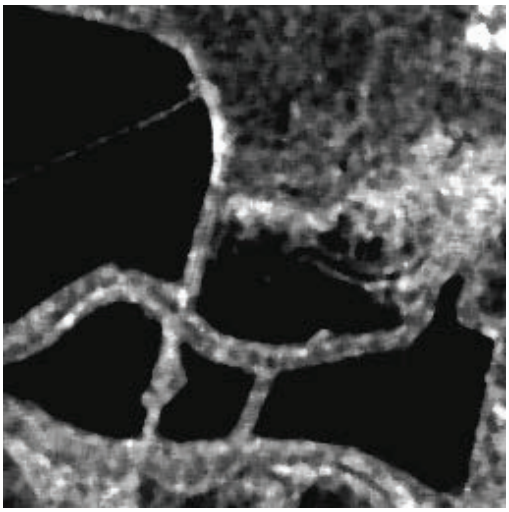

(b)

(c)

Fig. 1. San Francisco images (a) acquired in August 2003, (b) acquired in May 2004, and (c) map of changed areas (ground truth) used as a reference in simulations.

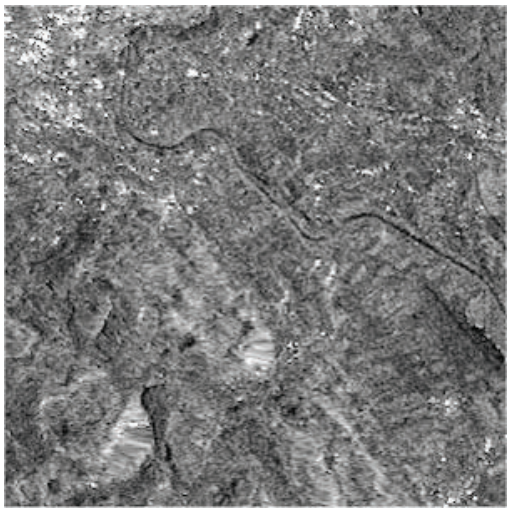

(a)

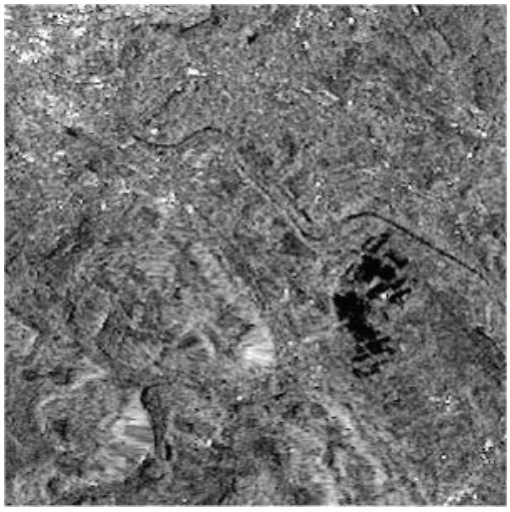

(b)

(c)

Fig. 2. The multiple-temporal SAR images of Bern city (a) acquired in April 1999, (b) acquired in May 1999, and (c) ground truth image.

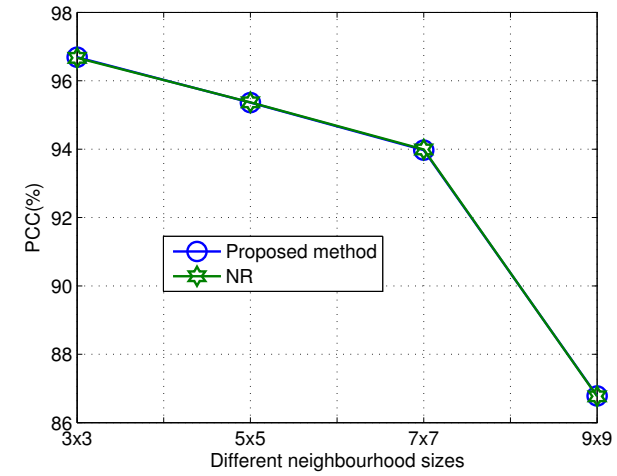

(a)

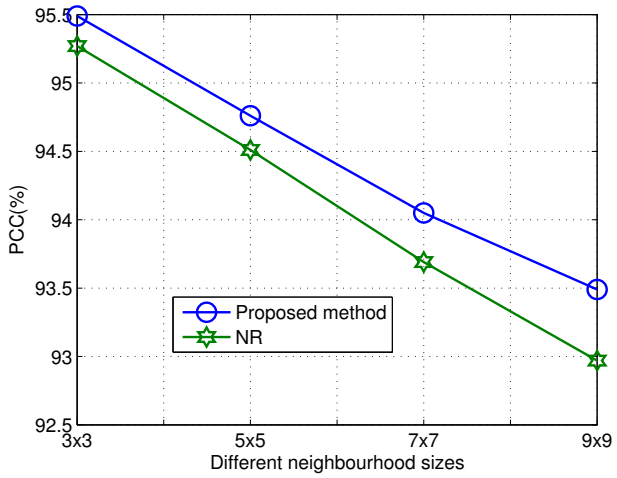

(b)

Fig. 3. The proposed algorithm was investigated with different neighbourhood sizes (a) for the images of San Francisco in Fig. 1, and (b) for the images of Bern city in Fig. 2. The filter was not applied in this case

For the first step, the neighbourhood sizes were changed from 3×3 to 9×9 pixels. For the neighbourhood size larger than 9×9 pixels, the results of the change detection of the two images can be incorrect. The reason is that the image patches are too smoothed, so heterogeneous factors seem to be the same. For each neighbourhood size, the proposed method without using post-filters and the NR method were simulated. The simulation results of the proposed method and the NR method with the different neighbourhood sizes were shown in Fig. 3. As can be seen in Fig. 3, the simulation results of the proposed method and the NR method are approximately the same in terms of PCC for the San Francisco (SF) images shown in Fig. 2 (see Fig. 3a) , while the proposed method is better than the NR one for the investigated images of Bern city (BC) shown in Fig. 2 (see Fig. 3b). For the both datasets of images investigated, the neighbourhood size of 3×3 pixels

provides the best result for these two methods. For instance, it can be seen from Table. I, for the optimal neighbourhood size of 3 × 3 pixels, the PCCs for the simulation results of proposed method and NR method with the SF image were approximately the same, 96.69 % and 96.67 %, respectively. For the BC image, the proposed method provided the accuracy higher 0.22 % than that of the NR algorithm; for instance, PCC of 95.49 % in comparison with PCC of 95.27 %.

TABLE I
THE SIMULATION RESULTS FOR THE PROPOSED METHOD AND THE NEIGHBOURHOOD BASED RATIO METHOD (NR) WITH THE NEIGHBOURHOOD SIZE OF 3X3 PIXELS

Images	SF	SF	BC	BC
Algorithms	The proposed	NR	The proposed	NR
PCC (%)	96.69	96.67	95.49	95.27

For the second step, for each neighbourhood size investigated in the first step, the proposed method was performed with using the average filters with different sizes changed from 3 × 3 to 9 × 9 pixels. The simulation results were shown in Fig. 4. As can be seen from Fig. 4 that the filter size of 7 × 7 pixels and the neighbourhood size of 3 × 3 pixels are the optimal combination for the proposed method for the both sets of images investigated. It can be seen from Table. II, this combination provided the PCCs of 98.55 % and 99.26 % for the San Francisco (SF) and Bern city (BC) images, respectively. These results were respectively higher 1.88 % and 3.99 % than those of the NR algorithm.

TABLE II
THE SIMULATION RESULTS FOR THE PROPOSED METHOD AND THE NEIGHBOURHOOD BASED RATIO METHOD (NR) WITH THE NEIGHBOURHOOD SIZE OF 3 × 3 PIXELS AND FILTER SIZE OF 7 × 7 PIXELS

Images	SF	SF	BC	BC
Algorithms	The proposed	NR	The proposed	NR
PCC (%)	98.55	96.67	99.26	95.27

In summary, the proposed method without using post-filters provided the change detection accuracy slightly higher than that of the NR algorithm [15]. By investigating the different neighbourhood and filter sizes through Matlab simulation, the optimal combination between them was found. The proposed method with the obtained optimal combination of these two parameters provided the change detection accuracy higher than that in the case without using post-filters, and higher than that of the NR algorithm.

IV. CONCLUSION

The paper developed a novel change detection in SAR images based on the averaged heterogeneous factors of the neighbourhood areas in the two multiple-temporal SAR images to create the difference image. The resultant difference image was then filtered by the average filter to reduce the speckle noises and to create the final change map. The different neighbourhood sizes and filter sizes were investigated to provide the optimal combination of these two parameters.

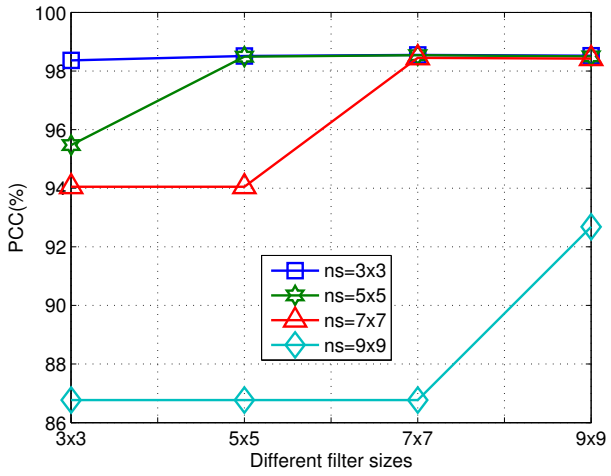

(a)

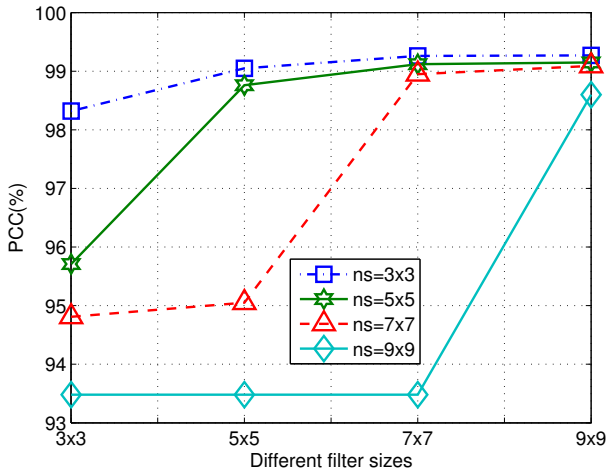

(b)

Fig. 4. The proposed algorithm was investigated with different filter sizes and neighbourhood sizes (ns) (a) for the images of San Francisco in Fig. 1, and (b) for the images of Bern city in Fig. 2.

The results of performance evaluation based on the Matlab simulation showed that the proposed method improved change detection accuracy in comparison with the the neighbourhood based ratio algorithm. In the near future, our research orientation will focus on simplifying computational procedures to increase processing speed of our change detection.

REFERENCES

[1] I. Onur, D. Maktav, M. Sari, and N. Kemal Sönmez, "Change detection of land cover and land use using remote sensing and gis: a case study in kemer, turkey," *International Journal of Remote Sensing*, vol. 30, no. 7, pp. 1749–1757, 2009.

[2] C. B. Hasager, M. Badger, A. Peña, X. G. Larsén, and F. Bingöl, "Sar-based wind resource statistics in the baltic sea," *Remote Sensing*, vol. 3, no. 1, pp. 117–144, 2011.
[3] N. Longbotham, F. Pacifici, T. Glenn, A. Zare, M. Volpi, D. Tuia, E. Christophe, J. Michel, J. Inglada, J. Chanussot *et al.*, "Multi-modal change detection, application to the detection of flooded areas: Outcome of the 2009–2010 data fusion contest," *IEEE Journal of selected topics in applied earth observations and remote sensing*, vol. 5, no. 1, pp. 331–342, 2012.
[4] Z. Liu, G. Li, G. Mercier, Y. He, and Q. Pan, "Change detection in heterogenous remote sensing images via homogeneous pixel transformation," *IEEE Transactions on Image Processing*, vol. 27, no. 4, pp. 1822–1834, 2017.
[5] F. Huang, L. Chen, K. Yin, J. Huang, and L. Gui, "Object-oriented change detection and damage assessment using high-resolution remote sensing images, tangjiao landslide, three gorges reservoir, china," *Environmental earth sciences*, vol. 77, no. 5, pp. 1–19, 2018.
[6] F. Bioresita, A. Puissant, A. Stumpf, and J.-P. Malet, "A method for automatic and rapid mapping of water surfaces from sentinel-1 imagery," *Remote Sensing*, vol. 10, no. 2, p. 217, 2018.
[7] F. Bovolo and L. Bruzzone, "The time variable in data fusion: A change detection perspective," *IEEE Geoscience and Remote Sensing Magazine*, vol. 3, no. 3, pp. 8–26, 2015.
[8] S. Hachicha and F. Chaabane, "On the sar change detection review and optimal decision," *International Journal of Remote Sensing*, vol. 35, no. 5, pp. 1693–1714, 2014.
[9] N. Otsu, "A threshold selection method from gray-level histograms," *IEEE transactions on systems, man, and cybernetics*, vol. 9, no. 1, pp. 62–66, 1979.
[10] J. Kittler and J. Illingworth, "Minimum error thresholding," *Pattern recognition*, vol. 19, no. 1, pp. 41–47, 1986.
[11] A. Singh, "Review article digital change detection techniques using remotely-sensed data," *International journal of remote sensing*, vol. 10, no. 6, pp. 989–1003, 1989.
[12] E. J. Rignot and J. J. Van Zyl, "Change detection techniques for ers-1 sar data," *IEEE Transactions on Geoscience and Remote sensing*, vol. 31, no. 4, pp. 896–906, 1993.
[13] C. Oliver and S. Quegan, *Understanding synthetic aperture radar images*. SciTech Publishing, 2004.
[14] Y. Bazi, F. Melgani, L. Bruzzone, and G. Vernazza, "A genetic expectation-maximization method for unsupervised change detection in multitemporal sar imagery," *International Journal of Remote Sensing*, vol. 30, no. 24, pp. 6591–6610, 2009.
[15] M. Gong, Y. Cao, and Q. Wu, "A neighborhood-based ratio approach for change detection in sar images," *IEEE Geoscience and Remote Sensing Letters*, vol. 9, no. 2, pp. 307–311, 2011.